Targeted Rework of Powder Bed Fusion Additive Manufacturing

Paul Dryburgh[1,*], Rikesh Patel[1], Sam Catchpole-Smith[2], Matthias Hirsch[2], Luke Parry[3], Richard J Smith[1], Matt Clark[1], Ian A Ashcroft[3] and Adam T Clare[2]

[1] Optics and Photonics Research Group
[2] Advanced Component Engineering Laboratory (ACEL)
[3] Centre for Additive Manufacturing (CfAM)
Faculty of Engineering, University of Nottingham, Nottingham, UK.

There is a clear industrial pull to fabricate high value components using premium high temperature aerospace materials by additive manufacturing. Inconveniently, the same materials' properties which allow them to perform well in service render them difficult to process via powder bed fusion. Current build systems are characterised by high defect rates and erratic microstructure, leading to components with inferior mechanical properties. Given the high specific costs in powder bed fusion manufacture there is a real and apparent need to minimise component scrappage due to these defects. Here a method is proposed to make good the defects that will inevitably be produced in current class laser processing of metallic powders.

This study investigates the use of spatially resolved acoustic spectroscopy (SRAS) scan data to inform repair strategies within a commercial selective laser melting machine. Using the common aerospace nickel superalloys, Inconel 718 and CM247-LC, localised re-melting was shown to consistently reduce the depth of defect. A 50 % reduction in defect depth was observed for both materials using different rework strategies. No appreciable variation was seen with the single-shot strategy, due inaccurate realignment.

Keywords: Powder bed fabrication, repair, rework, in-process monitoring, texture, laser processing

1. Introduction

Powder-Bed Fusion (PBF) additive manufacturing promises to herald a new age in design flexibility for high integrity applications, removing many traditional design constraints [1]. However, the levels of defects observed in current-class build systems is not acceptable to high-value industries. Current work-flows rely on post-fabrication inspection to assess integrity – unsurprisingly when combined with the defect rates seen in PBF this leads to significant component scrappage. An illustration of the PBF deposition process is shown in Figure 1, defects can form from the melt pool, ejected spatter or direct vaporisation from laser irradiation. The inherently stochastic nature of PBF makes defect formation inevitable. Optimisation of processing parameters is often a trade-off between key-holing, large in size with high aspect ratio, and metallurgical porosity, smaller and circular [2].

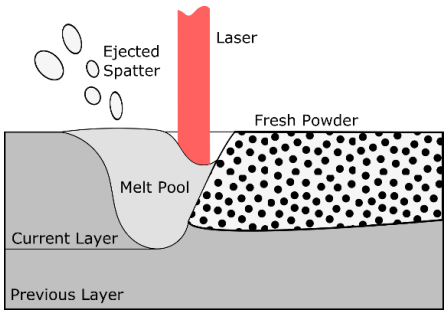

Figure 1 Basic process involved in powder-bed fabrication (PBF) to produce a component.

Undertaking in-line geometrical measurements, condition monitoring and intra layer integrity evaluation are therefore key aspects for pushing additive manufacturing forward and assuring that parts are of the required quality [3, 4]. Many of the Non-Destructive Evaluation (NDE) approaches to gain industrial traction generate optical datasets which can be used to identify surface defects [5]. One approach uniquely positioned to address many of the challenges posed by quality assurance in PBF is Spatially Resolved Acoustic Spectroscopy (SRAS). An acoustic microscopy technique, based on laser ultrasonics, the use of SRAS for additive manufacturing has been discussed in previous literature, and the appropriateness can be summarised by SRAS' ability to detect and differentiate between surface and subsurface defects [6], make informative measurements of the texture which can be correlated to build parameters [7], and the capability to measure off rough surfaces [8]. The continuing ambition is to develop the instrumentation into a system appropriate for integration with-in a build system, in order to capture acoustic data during fabrication.

Given the high specific cost of PBF components [9], a current field of research involves improving the properties of as-built components, avoiding scrappage. Current approaches on improving as-built density focus on full layer re-melting, however this has been shown to have undesirable effects on the tailored microstructure [10], and significantly increase processing time [11].

This study proposes a framework to combine these two parallel branches of research by investigating the potential of utilising data output from an NDE system to inform a rework operation to correct the defects that will inevitably be

produced in current class laser processing of metallic powders. By minimising additional build time, maintaining tailored microstructure and crucially avoiding component scrappage, localised rework of observed defects will represent a step change in machine tool technology.

2. Methodology

2.1 Spatially Resolved Acoustic Spectroscopy

Spatially Resolved Acoustic Spectroscopy (SRAS) is a laser-based acoustic microscopy technique used for material characterisation. A broadband Q-switched laser is imaged on to a sample, through a fringed optical mask with a known spacing, λ_g, allowing the temporal frequency content to be matched to the spatial frequency content of the sample. Surface acoustic waves are then generated through thermoselastic expansion, without damage to the sample surface. When the inspection wavelength used is much smaller than the sample thickness, $\lambda_g \ll t$, Rayleigh SAWs are generated. The Rayleigh wave has the useful property of being non-dispersive, meaning the propagation frequency remains constant along the propagation length, f_s. Unlike traditional time-of-flight measurements, the detection spot can be located at an arbitrary distance, and across multiple grain boundaries, from the generation patch, without affecting measurement fidelity.

A second laser and knife-edge detector is used to sense the surface perturbation caused by the propagation of the SAW. This perturbation occurs at the frequency of the acoustic wave. From the equation $v_{SAW} = f_s\lambda_g$, the velocity of the wave packet, at the generation patch can be calculated. The velocity an acoustic wave is directly related to the mechanical properties of the sample. Li et al. have reported on the use of the SRAS technique for recovering crystalline orientation information in large grain polycrystalline materials [12].

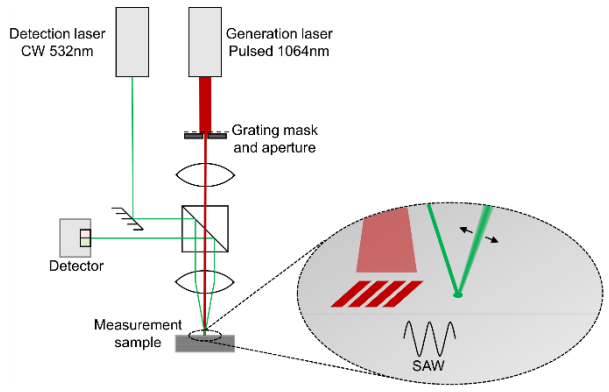

Figure 2 Set-up and instrumentation used in current iteration of SRAS system. Figure shows the generation and detection of a SAW.

The current iteration of the instrumentation, set-up shown in Figure 2, uses a 1064 nm (near infrared) laser (AOT-YAG-10Q) with 1-2 ns pulse length, giving frequency content up to 500 MHz, for generation. A 532 nm continuous wave laser (Laser Quantum Torus), with power of 200 mW is used for detection.

For this study an acoustic wavelength of 16 µm was selected, this leads to a generation patch size of ~120 µm and effective acoustic resolution of ~60 µm. In addition to obtaining velocity information, the system recorded an optical dataset of the measured surface; the image resolution being 10 µmpx^{-1} for rework vector generation.

2.2 Materials

For this study, two sets of samples had been fabricated, using the two aerospace nickel superalloys Inconel 718 and CM247-LC. All samples were manufactured using a Realizer SLM50 fabrication system, with processing parameters as given in Table 1.

Table 1 Processing parameters for sample fabrication

Parameter	Unit	Inconel 718	CM247-LC
Layer height	µm	40	40
Laser power	W	100	80
Scan speed	mms^{-1}	560	600
Hatch spacing	µm	60	40
Energy	nJm^{-3}	75.8	83.3

Whilst both materials are of significant interest to PBF research, CM247-LC is a more challenging material to process due to its 'unweldable' nature, leading to solidification cracking. This occurs in the weld metal during the terminal stages of solidification when a liquid film is distributed along grain boundaries and inter-dendritic regions - the shrinkage strains across these boundaries cannot be accommodated [13].

All samples were polished using standard metallographic preparation, giving a final surface roughness <100 nm to facilitate optical inspection. In order to evaluate the defect depth, point cloud micrographs were captured using a focus variation microscope (Alicona InfiniteFocus G5) with a 20× lens and in-built image stitching tool. The lateral and vertical resolution of the 3D micrographs was 2.94 µmpx^{-1} and 0.1 µmpx^{-1}, respectively.

2.3 Repair vector generation

One of the fundamental components to the framework presented in this study, is the use of measured data as an input for generating repair vectors. In a real manufacture scenario, measurements would be captured simultaneously with deposition. However, in order to study the rework process using external tools such as SRAS, the sample is manufactured, analysed and then returned to the build system for rework.

Given the irregular morphology of defects found in PBF, morphological closing and smoothing operations are performed on the data before generation of repair vectors. This is also used to group closely congregated defects into one rework area to prevent interference from attempting to rework separately. Figure 3(a) shows the SRAS optical map of the Inconel 718 surface, used as an input for generation of rework vectors. Figure 3(b) highlights a large defect in the sample, after morphological closing has been applied. Finally, Figure 3(c) shows the actual laser scan vectors that were applied to enact rework in this area. The angle of the vectors was intended to follow the major dimension of the defect, and moves from left to right across the sample. The repair area length was 150% of each defect major axis length.

The methodology presented for generation of rework vectors is deliberately generalised to make the approach applicable to a wide range of in-line monitoring techniques.

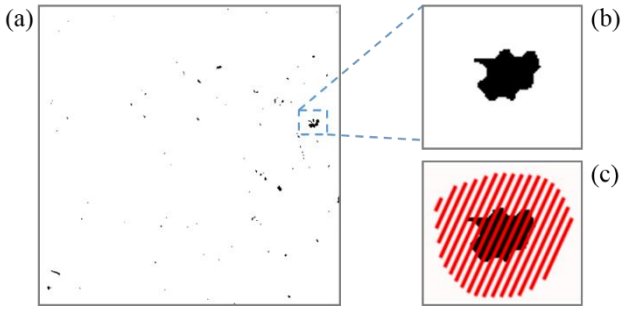

Figure 3 Optical image of Inconel 718 sample captured using SRAS, on a binary scale, indicating surface breaking defects.

Three approaches to rework have been proposed, and trialled in this study: hatch, spiral and single-shot, as shown in Figure 4. The spiral melting pattern was proposed by Jhabvala et al., showing optimised thermal gradients in both the *x* and *y* direction designed to avoid overheating [14]. The indicted size of single shot defects are significantly smaller, as this approach is reserved for defects smaller than the laser beam diameter, < 40 µm.

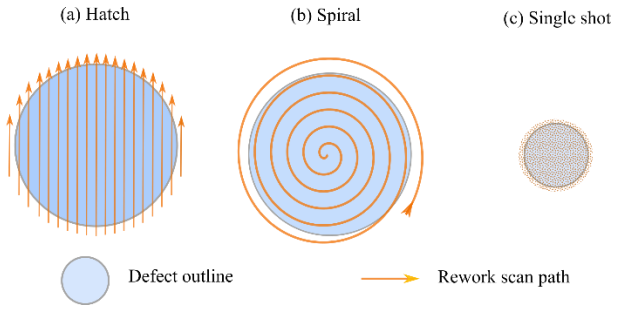

Figure 4 Rework strategies trialed in this study

3. Rework of Inconel 718

Considering first the Inconel optical map shown in Figure 3(a), the majority of observed defects can be classified as key-holing, rather than metallurgical. These defects normally stem from under-melting or spatter, and unlike metallurgical defects, create voids with irregular shapes that can be key stress concentration sites [2, 15]. Exemplary micrographs of these defects are given in Figure 6 (a) – (d), and the corresponding reworked areas in Figure 6 (e) – (h). Figure 6 (a) and (e) shows the defect initially highlighted in Figure 3. From the micrographs, it can be qualitatively seen that the rework has reduced the variation in surface height due to the defect, and eliminated the high-aspect ratio features that are characteristic of key-hole defects. For a quantitative study, profile measurements are taken across the total re-melted area – the lowest points comparing pre- and post- rework are shown in Figure 5. A reduction in variance can be observed for hatch and spiral rework patterns. The single shot rework patterns show no statistically relevant improvement.

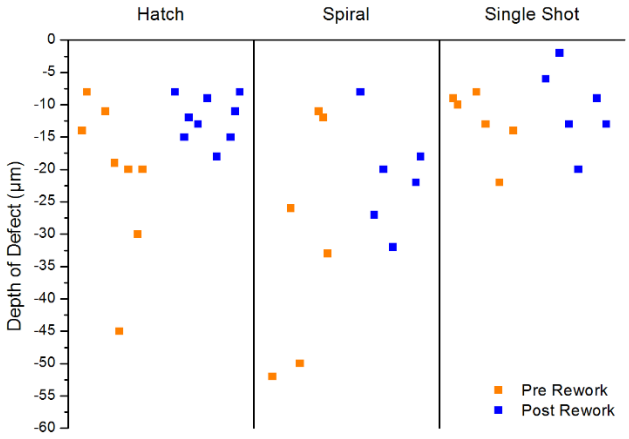

Figure 5 Comparison of defect depth pre- and post-rework for each repair strategies in Inconel 718.

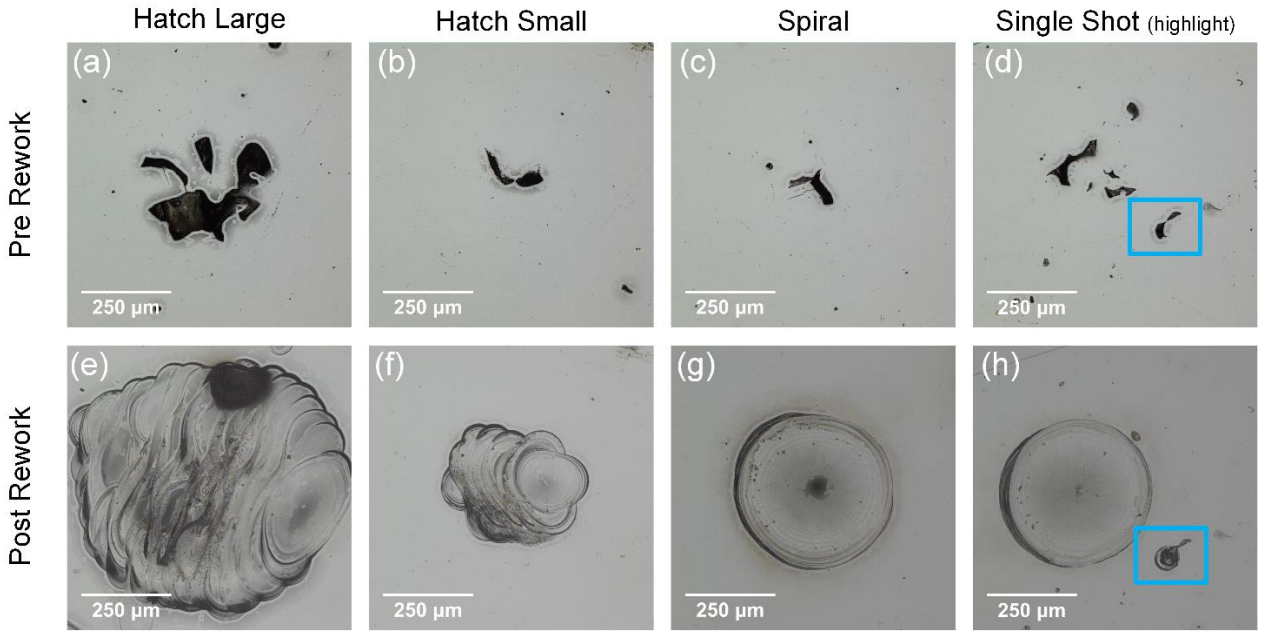

Figure 6 Micrographs showing pre- (a-d) and post- (e-h) rework defects, for the three scan strategies trialled, in Inconel 718.

4. Rework of CM247-LC

Figure 7 shows isometric micrographs of a typical PBF fabricated CM247-LC sample – etching reveals the microstructure and characteristic micro-cracking.

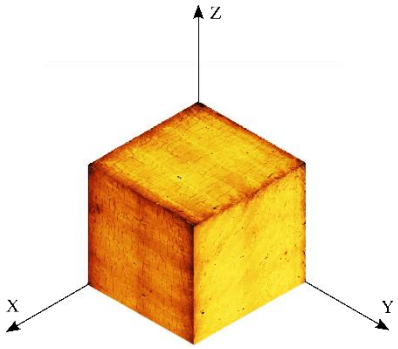

Figure 7 Etched isometric micrographs of typical CM247-LC PBF microstructure and micro-cracking.

Again the three strategies, as defined in Figure 4, are trialled in CM247-LC samples. Figure 8 compares the maximum variation in height across the re-melted zone. The magnitude of each bar indicated the population standard deviation. In both cases it can be seen that there is a significant reduction in the standard deviation in height across the reworked area. Interestingly both techniques appear to have a similar lower limit, ~18 µm, but the hatch approach has a lower upper bound, ~24 µm compared to ~35 µm. Although initial defects reworked with the spiral approach have a much wider distribution, this may not be a fair comparison. Overall, it is clear that rework is again successful in reducing the variation in height caused by surface breaking defects. Single shot repairs have not been included in this analysis as the realignment error was significantly larger in the CM247-LC samples, preventing meaningful analysis.

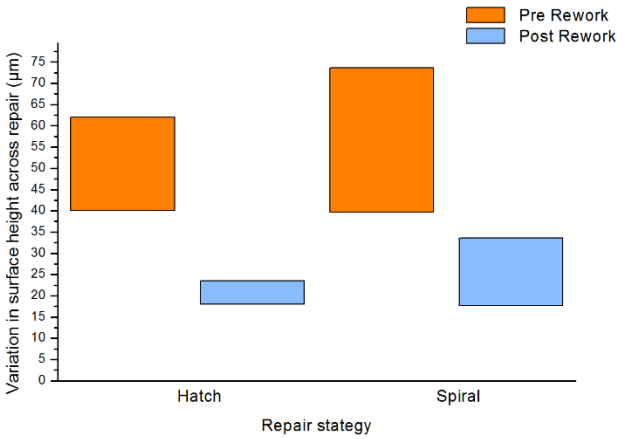

Figure 8 Comparison of maximum variation in height across defect depth pre- and post-rework for each hatch and spiral strategies in CM247-LC.

Figure 9 shows exemplary micrographs of reworked zones in CM247-LC for each rework strategy. The most notable feature is the cracking propagating from the centre of the re-melted zone. Observed cracking exhibits a 'jagged' nature, similar to those reported by Carter et al. in high energy fabrication, where the dendritic growth suggests crack initiation during solidification [16].

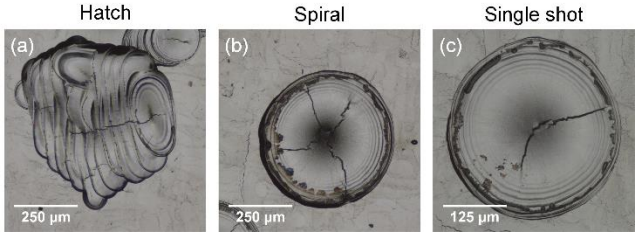

Figure 9 Micrographs of exemplary cracking in CM247-LC, after rework for each trialled strategy.

5. Discussion

Considering all of the datasets presented, it is clear that the process of rework has consistently decreased the depth of the defect, nominally within the depth of one layer. A reduction in the depth of the defect along with a profile more favourable for infill with powder in the next build layer means that if such reworks are performed in-situ as defects develop, conditions are favourable for powder filling the defect in the next layer and the avoidance of the defect propagating through multiple layers.

In the Inconel sample, spiral rework shows an improvement of 31% and 50% for the hatched pattern. In CM247-LC both methods show a mean improvement of around 50%. Interestingly, both techniques appear to have a similar lower limit, 10 – 15 µm, suggesting this rework approach maybe more suitable for larger defects.

It is possible to compare the realised rework with the programmed vector from the micrographs captured after rework. Figure 10 shows a typical spiral rework in Inconel 718, with the intended rework vector overlaid to scale. Firstly, it is interesting to note the total re-melted area extends around 100 – 150 µm beyond the outer turn, this is in good agreement with previous reporting on melt pool size. This does mean however that as the vector spans 150 % of the initial defect, plus the 150 µm re-melted area – for even small defects there is a large impact on the surface. Furthermore, some slight cracking can be seen at the interface of the re-melted area and the bulk – this is seen in a minority of trialled reworks.

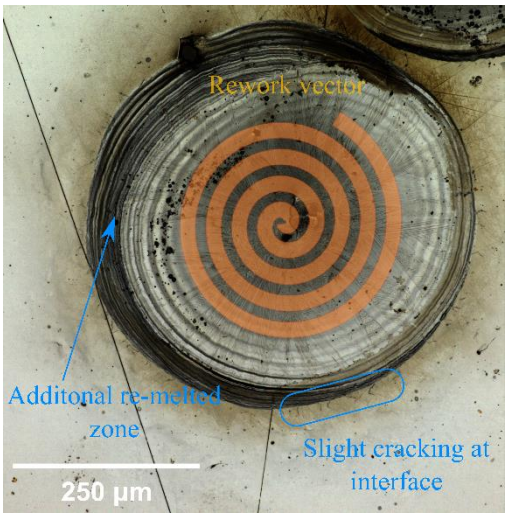

Figure 10 Micrograph of reworked area in Inconel 718, showing hatch re-melted zone, after subtle re-polishing to level surface (a) and etching to reveal microstructure (b).

Figure 11 shows a detailed SRAS velocity map taken from the area surrounding rework zone shown in Figure 10. Again, the intended vectors are indicated (orange spiral), along with the apparent total size of re-melted zone (blue circles). Some areas of the re-melted zone could not be imaged due to the roughness caused by reworking. Again, it is clear that the re-melted zone extends significantly beyond the outer vector. One of the key characteristics of Nickel is its wide acoustic wave velocity range (due to elastic anisotropy), however a re-melted zone is known to have a cellular/dendritic microstructure is more homogenous and has a smaller cell size than found in the as-deposited PBF sample [17]. Looking at the bulk of the sample, the measured texture is similar to previously reported nickel PBF samples [7], suggesting the rework action has had little to no impact on the bulk of the material. This satisfies the aim of minimising the effect on the microstructure with targeted rework. Looking at the area within the re-melted zone, there does appear to be some texture inheritance from the bulk but this may be attributed to the propagation direction of the acoustic waves. Additionally, towards the centre of the re-melted zone, there does appear to be some homogenising of texture, although accurate measurements have been obscured by the aforementioned surface roughness. Future reporting will contain a detailed discussion on the texture development within the reworked zone.

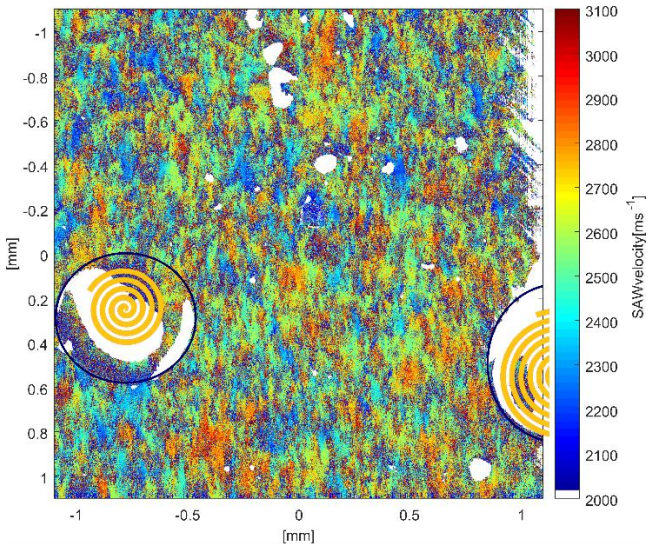

Figure 11 Detailed SRAS velocity map, taken from hatch re-melted zone in Inconel 718.

The observed cracking phenomena is concomitant with PBF processed CM247-LC due to its 'unweldable' nature [16]. A comparison of the crack length density, measured in the reworked zones, are comparable with measurements taken from the bulk, Figure 12. Whilst clearly such components are unsuitable for use in high integrity applications, research into improved build strategies for 'unweldable' in PBF continues [18]. The thermal cracking seen in Inconel 718 was unexpected as this is normally consider the easiest to process nickel superalloy, however previous studies have shown that cracks often occurred in the overlapping regions between laser scanning passes in superalloys, due to residual stress – this may be the cause of this interface cracking [19, 20].

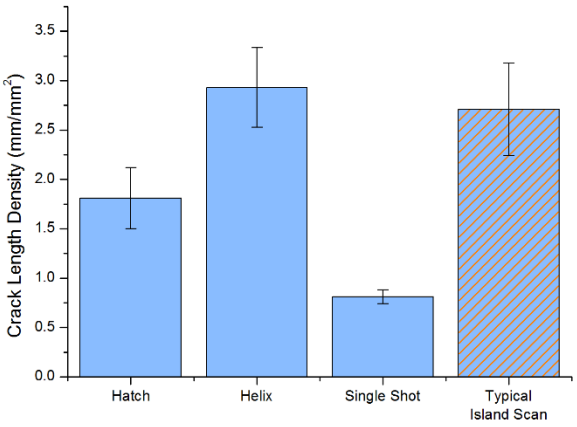

Figure 12 Crack length density comparison in CM247-LC.

Additionally, questions remain regarding the actual motion of the laser. The spiral and concentric repair patterns in particular, produce vectors with increasingly small motion. This relies on the precise control of the galvanometer scanning mirrors, however, in reality the laser likely does not complete the final few vectors, remaining fixed at the centre of the repair. This will cause over heating over the centre and may be a source of the crack radiating outwards from the centre, seen in the CM247-LC samples.

Generating repair vectors based on two dimensional data has the obvious drawback of neglecting the impact of defect depth. As material is continually moved towards the centre in circular-based methods, this can result in too much material being move in and a peak being formed at the centre of the rework zone. However, in the hatched repair, excess material is allowed to run off the edge of each vector. In an in-line solution, this may be negated by continual monitoring, meaning the depth of defect can be inferred from the layer height. An analogous effect can also be found in 2D with defects of varying cross-section. The spiral repair method, generates one circular repair area, however the hatched vector can vary length along a path, this is more readily demonstrated by observing a hypothetical hourglass shaped defect, and the corresponding repair areas, Figure 13. This is thought to be the source of the rise in surface height often seen at the centre of spiral re-worked areas, where too much material has been brought to too small a defect volume.

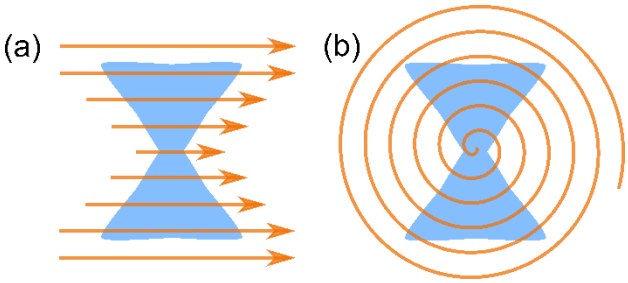

Figure 13 Hatching of exemplary 'hourglass style' defect. The hatch vectors are able to follow the morphology of the defect

Aside from the framework itself, one drawback of this study is the need to capture measurements offline, necessitating realignment within the build system, which inevitably induces positional errors, particularly noticed in the smaller ingle shot reworks. The authors continuing objective is to

fully integrate a SRAS system within a functional PBF build system, which will allow for these measurements and generation of repair vectors online – however significant challenges remain, primarily optical detection from a rough as-deposited surface.

6. Conclusion

The work presented in this paper has expanded upon laser re-melting beyond simply improving surface finish to investigate the feasibility of correction of surface defects, through NDE informed rework vectors. Results have shown targeted rework of nickel superalloy SLM component surfaces is a feasible approach to reducing porosity defects.

The key conclusions are as follows:

- Three laser scan strategies were trialled in order to rework non-artificial defects: hatch, spiral and one-shot (for defects below 40 µm).
- Some rework techniques were shown to successfully rework the pores and reduce the variation in depths across the defect, with the hatch technique proving to be the most effective – a defect depth improvement of 50% was achieved on average in both sample sets.
- No meaningful conclusions could be drawn on the single-shot approach due to difficulties in realignment of the sample within the build system for re-melting.
- The total re-melted zone extended an additional 100 to 150 µm outside of the vector, due to the size of the melt pool. This leads to large re-melted areas for even small defects, thus the 150% scaling should be decreased in future trials.
- Little texture influence on the bulk material due to re-melting should be seen, but this requires further analysis.

The methodology of rework demonstrated in this paper is highly suitable for integration into an entirely in-situ system, as measurements can be made within a modified SLM laser/optics system, rework scan paths can be computed on-the-fly, and the rework paths can be applied within the same manufacturing process with little increase in build time. Whilst this study has focussed on targeted surface rework, the advent of in-situ inspection would allow for re-melting to occur throughout the build-process in order to rework defects within the build volume of the component.

Acknowledgments and Appendixes

This work was supported by the Engineering and Physical Sciences Research Council [grant number EP/L022125/1] through the 'UK Research Centre in Non-Destructive Evaluation'. We would like to thank the Centre for Additive Manufacture for enabling us to fabricate the specimens.

References

1. Fousová, M., et al., *Promising characteristics of gradient porosity Ti-6Al-4V alloy prepared by SLM process.* Journal of the Mechanical Behavior of Biomedical Materials, 2017. **69**: p. 368-376.
2. Aboulkhair, N.T., et al., *Reducing porosity in AlSi10Mg parts processed by selective laser melting.* Additive Manufacturing, 2014. **1-4**: p. 77-86.
3. Caffrey, T., I. Campbell, and T. Wohlers, *Wohlers Report 2016: Additive Manufacturing and 3D Printing State of the Industry, Annual Worldwide Progress Report*. 2016: Wohlers Associates, Inc.
4. Everton, S.K., et al., *Review of in-situ process monitoring and in-situ metrology for metal additive manufacturing.* Materials and Design, 2016.
5. Everton, S.K., et al., *Review of in-situ process monitoring and in-situ metrology for metal additive manufacturing.* Materials & Design, 2016.
6. Smith, R.J., et al., *Spatially Resolved Acoustic Spectroscopy for Selective Laser Melting.* Journal of Materials Processing Technology, 2016.
7. Hirsch, M., et al., *Meso-scale defect evaluation of selective laser melting using spatially resolved acoustic spectroscopy.* Proc. R. Soc. A, 2017. **473**(2205): p. 170-194.
8. Sharples, S.D., et al., *The SKED: speckle knife edge detector.* Journal of Physics: Conference Series, 2014. **520**: p. 012004.
9. Baumers, M., et al., *The cost of additive manufacturing: machine productivity, economies of scale and technology-push.* Technological Forecasting and Social Change, 2016. **102**: p. 193-201.
10. Newton, T.R., et al., *Investigation of the effect of process parameters on the formation and characteristics of recast layer in wire-EDM of Inconel 718.* Materials Science and Engineering a-Structural Materials Properties Microstructure and Processing, 2009. **513-14**: p. 208-215.
11. Yasa, E. and J.P. Kruth, *Application of Laser Remellting Selective Laser Melting Parts.* Advances in Production Engineering and Management, 2011. **6**(4): p. 259-270.
12. Li, W., et al., *Determination of crystallographic orientation of large grain metals with surface acoustic waves.* J Acoust Soc Am, 2012. **132**(2): p. 738-45.
13. Dupont, J.N., J.C. Lippold, and S.D. Kiser, *Welding Metallurgy and Weldability of Nickel - Base Alloys*. 2009.
14. Jhabvala, J., et al., *On the effect of scanning strategies in the selective laser melting process.* Virtual and Physical Prototyping, 2010. **5**(2): p. 99-109.
15. Tammas-Williams, S., et al., *The Influence of Porosity on Fatigue Crack Initiation in Additively Manufactured Titanium Components.* Scientific Reports, 2017. **7**(1): p. 7308.
16. Carter, L.N., M.M. Attallah, and R.C. Reed, *Laser Powder Bed Fabrication of Nickel-Base Superalloys: Influence of Parameters; Characterisation, Quantification and Mitigation of Cracking*. 2012, John Wiley and Sons, Inc. p. 577-586.

17. Yasa, E., J. Deckers, and J.P. Kruth, *The investigation of the influence of laser re‐melting on density, surface quality and microstructure of selective laser melting parts.* Rapid Prototyping Journal, 2011. **17**(5): p. 312-327.
18. Catchpole-Smith, S., et al., *Fractal Scan Strategies for Selective Laser Melting of 'Unweldable' Nickel Superalloys.* Additive Manufacturing, 2017. **15**: p. 113-122.
19. Liu, F., et al., *Microstructure and residual stress of laser rapid formed Inconel 718 nickel-base superalloy.* Optics & Laser Technology, 2011. **43**(1): p. 208-213.
20. Yang, J., et al., *Experimental study on residual stress distribution of laser rapid forming process.* Rare Met Mater Eng, 2004. **12**: p. 1304-1307.